Supporting Information

Achieving ultrahigh synaptic potentiation with a two-terminal device based on a solution processed $Cs_3Bi_2Br_9$-MoS_2 hybrid

Xiaoyu Zhang,[aϕ] Jian Wang,[aϕ] Yanjun Liang,[a] Lu Jiang,[a] Zhiwei Yang,[a]
Jian Zhang*[a] and Xiao Huang*[a]

[a] *Institute of Advanced Materials (IAM), Nanjing Tech University (NanjingTech), 30 South Puzhu Road, Nanjing 211816, China.*

E-mail: iamjzhang@njtech.edu.cn, iamxhuang@njtech.edu.cn

Experimental Section

1. Experimental Materials

Cesium bromide (CsBr, purity 99.0%, Sigma Aldrich), bismuth bromide ($BiBr_3$, purity 99.0%, Aladdin), oleylamine (OLA, purity 80%~90%, Aladdin), oleic acid (OA, analytical grade, Aladdin), dimethyl sulfoxide (DMSO, analytical grade, Yonghua Chemical), molybdenum disulfide (MoS_2, purity 99.5%, Energy Chemical), isopropyl alcohol (IPA, purity 99%, Aladdin). All reagents were used directly without further purification.

2. Synthesis of $Cs_3Bi_2Br_9$ (CBB)

0.3 mmol CsBr and 0.2 mmol $BiBr_3$ were dissolved in a mixed solvent consisting of 5 mL DMSO, 30 μL OLA, and 0.6 mL OA. The mixture was stirred magnetically for 1 h to obtain a clear CBB precursor solution. Using the ligand-assisted reprecipitation method, 0.5 mL of the precursor solution was rapidly injected into 5 mL of IPA antisolvent under vigorous shaking and allowed to react statically for 1 min. Subsequently, the product was collected by centrifugation at 8000 r/min, and the precipitate was dispersed in IPA for subsequent characterizations.

3. Synthesis of CBB-MoS_2 Hybrid

MoS_2 nanopowder was dispersed in IPA, exfoliated by ultrasonication, and centrifuged. The supernatant was collected and dried under vacuum to obtain MoS_2 solid. 0.959 mmol of the dried MoS_2 was weighed and re-dispersed into the CBB precursor solution, followed by vigorous stirring for 1 h to ensure thorough mixing of the two components. Then, 0.5 mL of the mixed precursor solution was dropped into 5 mL of IPA. The product was collected by centrifugation, washed, and finally the CBB-MoS_2 hybrid material was obtained.

4. Device Fabrication

The device adopts a two-terminal structure by using an interdigitated Au electrode (planar bottom-electrode structure). The CBB-MoS_2 hybrid film was deposited onto the interdigitated Au electrode (interdigital spacing:100 μm) via drop-casting. The CBB-MoS_2 hybrid material and other control samples were drop cast onto commercial interdigitated gold electrodes (substrate dimensions: 10 mm × 20 mm, interdigital spacing: 0.05 mm, substrate material: Al_2O_3, purchased from Huizhou Xinwenxiong Trading Co., Ltd.).

5. Characterizations

The crystal structure and microstructure of the samples were characterized using X-ray diffraction (XRD, Rigaku Smartlab 3KW, Japan, Cu Kα radiation, λ = 1.54 Å), transmission electron microscopy (TEM, JEOL 2100 Plus, Japan), and high-resolution transmission electron microscopy (HRTEM, JEOL 2100F, Japan). Optical properties of the samples were analyzed using a UV-Vis spectrophotometer (UV-Vis, Shimadzu UV-1780, Japan), a photoluminescence spectrometer (PL, Hitachi F-7100, Japan), and a time-resolved photoluminescence spectrometer (TRPL, Edinburgh Instruments FLS-980, UK). The electronic structure characteristics of the samples were characterized using ultraviolet photoelectron spectroscopy (UPS, ThermoFisher Scientific Nexsa, USA) and X-ray photoelectron spectroscopy (XPS, Thermo Fisher Scientific K-Alpha, USA). During optoelectronic performance measurements, the illumination intensity and relative humidity were adjusted using a laser power meter (Sanwa LP10, Japan) and a hygrometer (Anymetre TH21E, China), respectively. Optoelectronic performance tests were completed using an electrochemical workstation (Autolab 86567, Switzerland), a laser source (Thorlabs DC2200, USA), and a semiconductor characterization system (Keithley 4200SCS, USA).

6. Neuromorphic computing simulation (MNIST)

MNIST handwritten digit recognition was simulated using NeuroSimV3.0 with a fully-connected two-layer multilayer perceptron (MLP) consisting of 400 input neurons, 100 hidden neurons, and 10 output neurons. The 28×28 MNIST images were flattened into 400-dimensional input vectors. The network was trained for 35 epochs using [cross-entropy loss] and [SGD/NeuroSim default] settings. The measured ΔPSC evolution under light pulses was discretized into 15 conductance states:G_1, G_2, ... G_{15}. The normalized weight was defined as $\omega = (G - G_{min})/(G_{max} - G_{min})$. Signed synaptic weights were implemented using a differential-pair scheme: $W = (G_p - G_m)/(G_{max} - G_{min})$, where G_p and G_m follow the experimentally extracted potentiation and depression trajectories respectively. During training, the gradient sign selects potentiation (increase G_p/decrease G_m) or depression (decrease G_p/increase G_m). Each update corresponds to a one-step transition between adjacent conductance states to reflect the discrete nature of device programming.

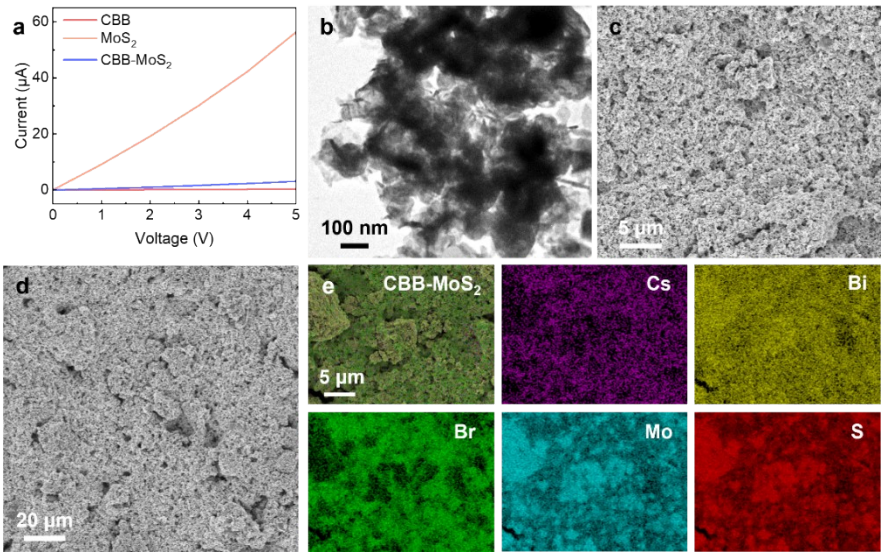

Fig. S1 (a) I-V characteristics of pure CBB, MoS_2, and CBB-MoS_2. (b) TEM, (c) high magnification SEM and (d) large area SEM images of CBB-MoS_2 hybrid film. (e) EDS elemental mapping images of CBB-MoS_2 hybrid film.

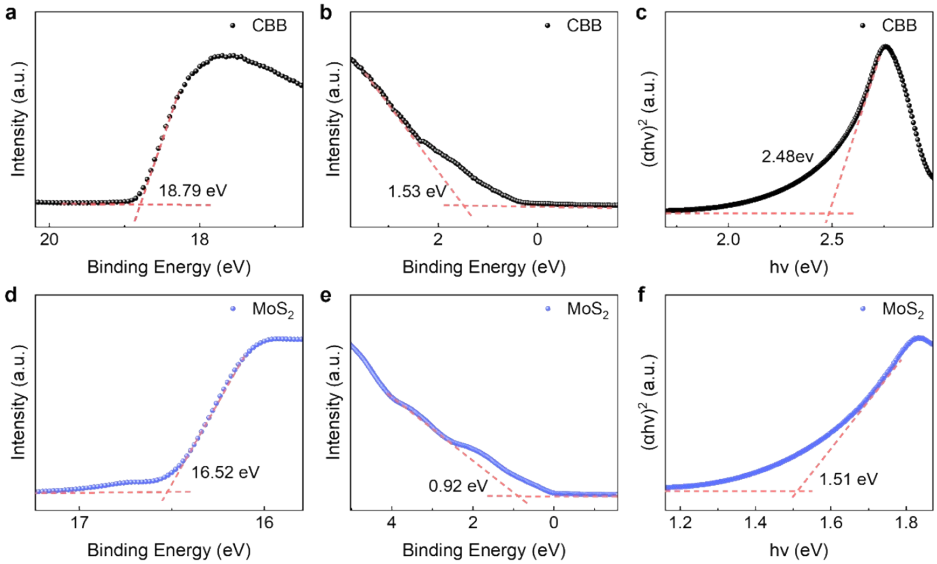

Fig. S2 (a-b) UPS analysis of CBB. (c) Tauc plot of CBB. (d-e) UPS analysis of MoS_2. (f) Tauc plot of MoS_2.

According to the UPS and Tauc analysis (Fig. S2), the VBM and CBM positions of CBB and MoS_2 give rise to a staggered band alignment at the heterointerface, which upon light excitation, promotes photogenerated electrons and holes to preferentially transfer from CBB to MoS_2.

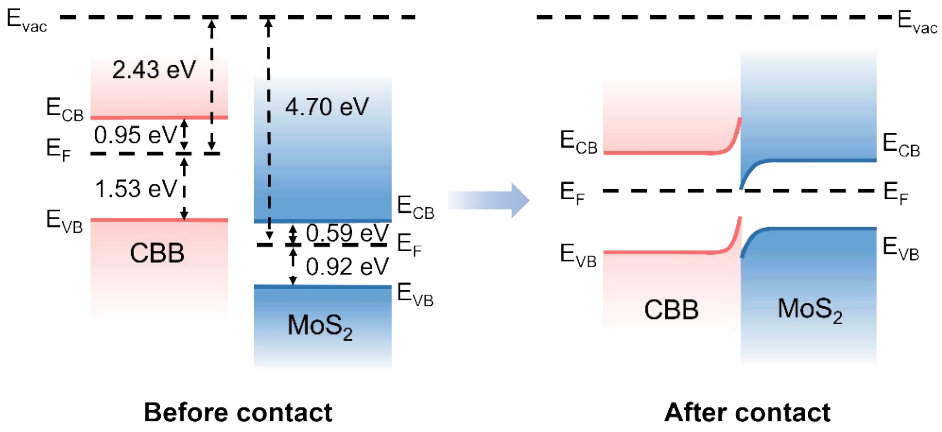

Fig. S3 Schematic diagram of the band alignment before and after formation of CBB-MoS_2 heterojunction.

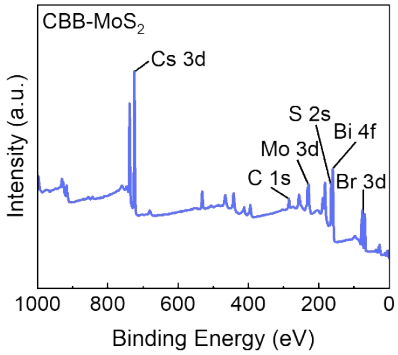

Fig. S4 XPS survey spectrum of the CBB-MoS_2 hybrid.

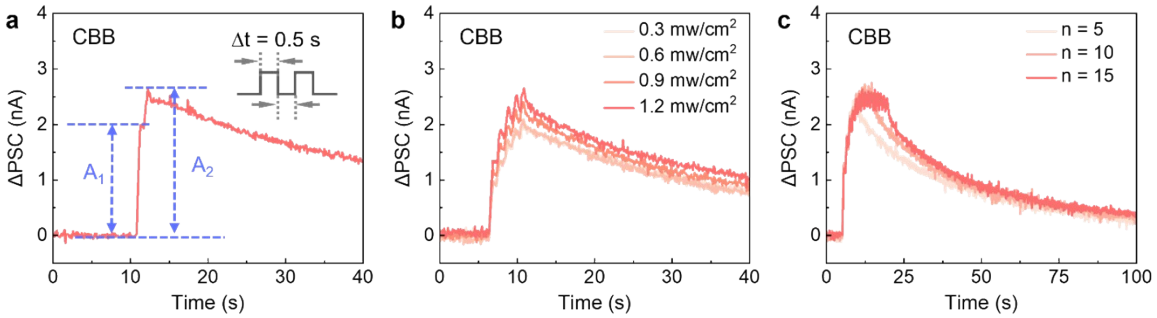

Fig. S5 (a) The change of excitatory postsynaptic current of CBB device triggered by two consecutive optical pulses. (b) The change of excitatory postsynaptic currents of the CBB device measured under various optical powers. (c) The change of excitatory postsynaptic currents of the CBB device measured with increasing pulse numbers.

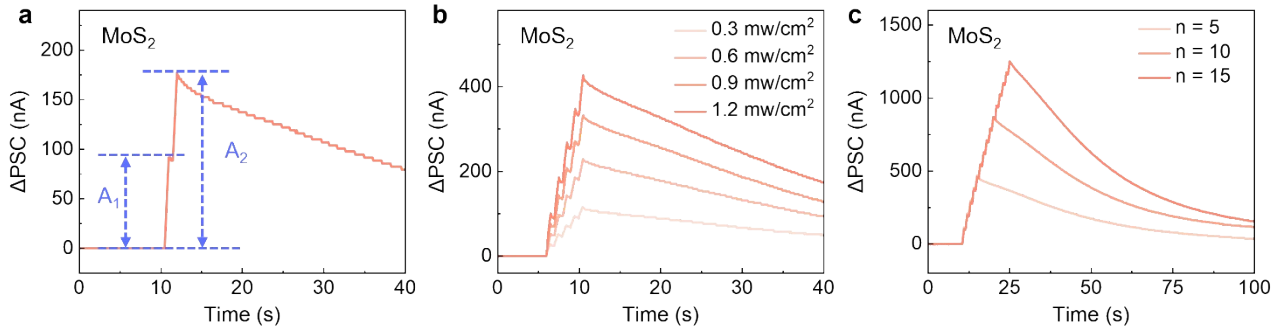

Fig. S6 (a) The change of excitatory postsynaptic current of MoS_2 device triggered by two consecutive optical pulses. (b) The change of excitatory postsynaptic currents of the MoS_2 device measured under various optical powers. (c) The change of excitatory postsynaptic currents of the MoS_2 device measured with increasing pulse numbers.

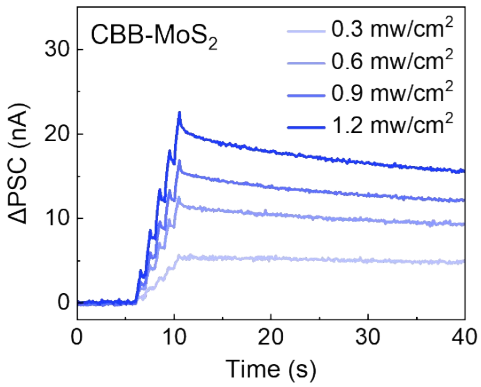

Fig. S7 The change of excitatory postsynaptic currents of the CBB-MoS_2 device measured under various optical powers.

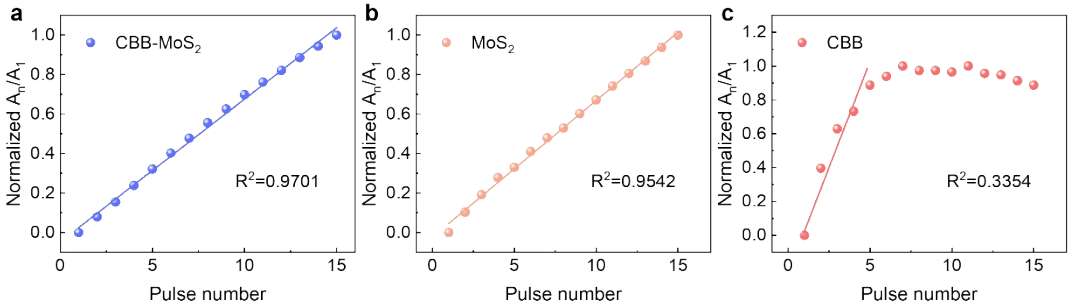

Fig. S8 Linear fitting of the weight update (A_n/A_1) plots of (a) CBB-MoS_2, (b) MoS_2 and (c) CBB based devices.

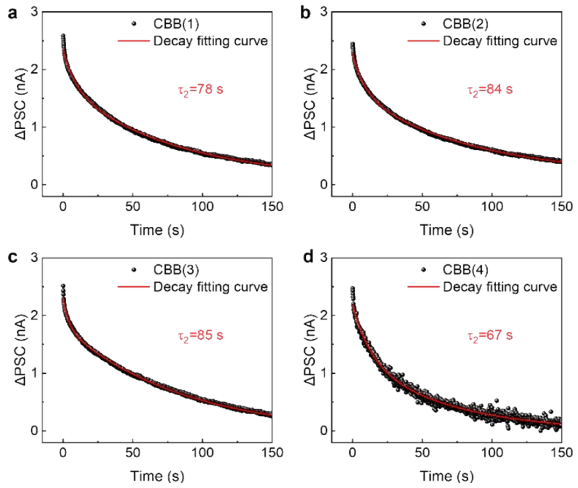

Fig. S9 The ΔPSC decay curves of four independent CBB devices after 15 consecutive optical pulses, along with their corresponding double-exponential fitting curves.

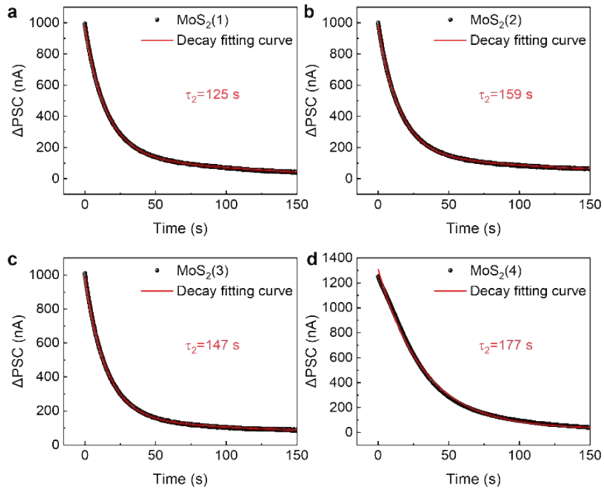

Fig. S10 The ΔPSC decay curves of four independent MoS_2 devices after 15 consecutive optical pulses, along with their corresponding double-exponential fitting curves.

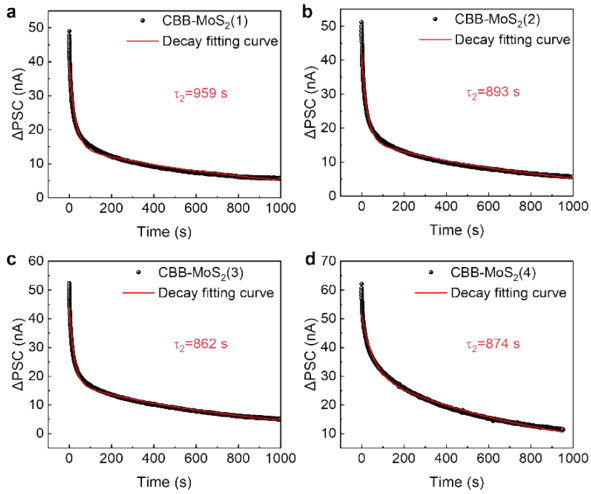

Fig. S11 The ΔPSC decay curves of four independent CBB-MoS_2 devices after 15 consecutive optical pulses, along with their corresponding double-exponential fitting curves.

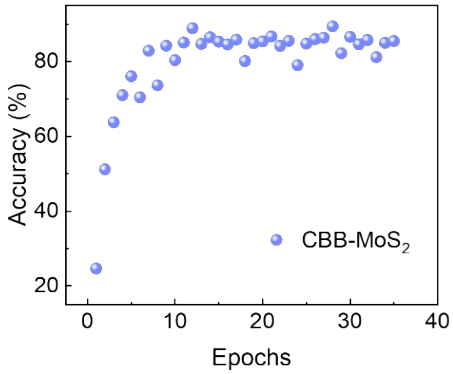

Fig. S12 Accuracy calculation of the network based on CBB-MoS_2 under realistic noise conditions.

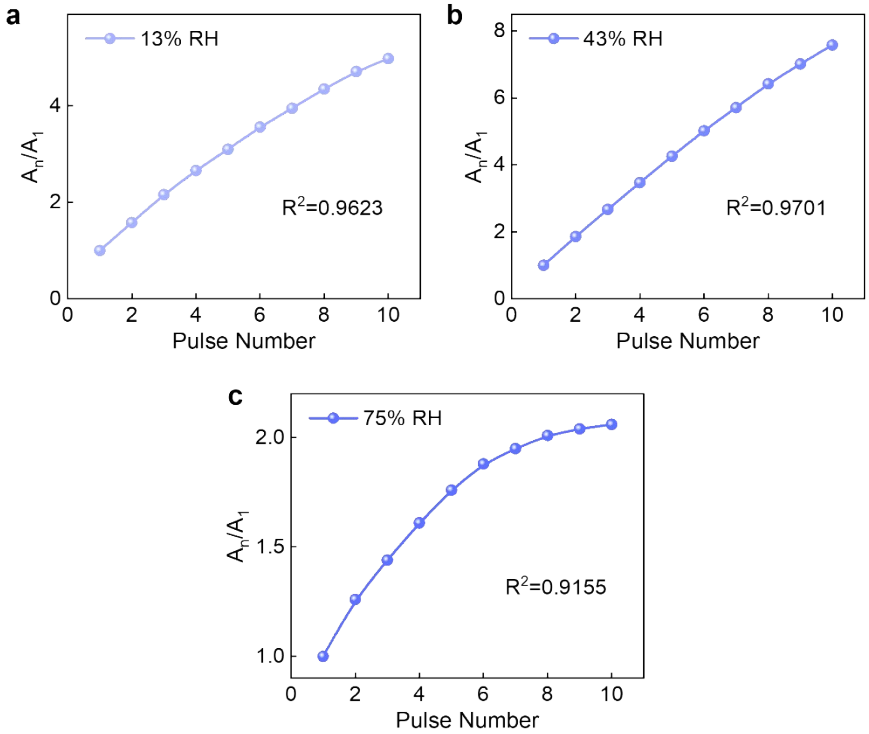

Fig. S13 Comparison of linearity of weight update (A_n/A_1) of the CBB-MoS_2 device at various relative humidity levels: (a) 13% RH, (b) 43% RH, (c) 75% RH.

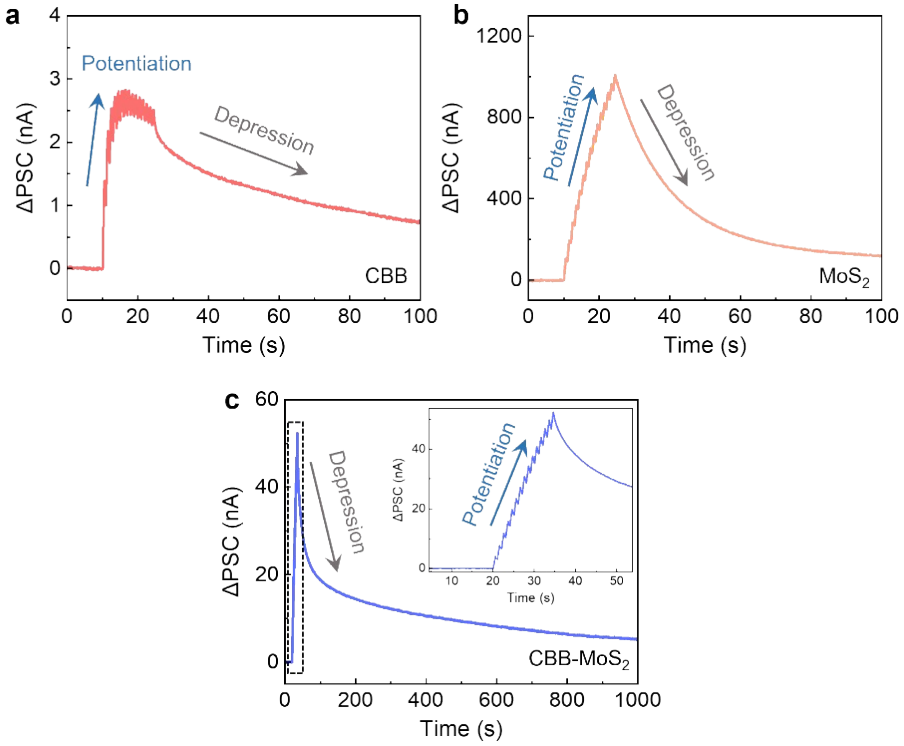

Fig. S14 Depression behaviors of (a) CBB, (b) MoS_2, and (c) CBB-MoS_2 based devices.

Table S1 Comparison of PPF index and recognition accuracy of our device with previously reported three-terminal synaptic devices.

Ref.	Device Type	PPF Index	Image Recognition Accuracy
This work	**Two-terminal**	**230%**	**96%**
[1]	Three-terminal	187%	91.4%
[2]	Three-terminal	160%	91.07%
[3]	Three-terminal	180%	92.05%
[4]	Three-terminal	153%	98.8%
[5]	Three-terminal	170%	92.88%
[6]	Three-terminal	172%	93.88%

Table S2 Symmetry factors of CBB, MoS_2 and CBB-MoS_2 based devices.

Material	CBB	MoS_2	CBB-MoS_2
Symmetry factor	0.819	0.52	0.685

$$ANL = \frac{G_{LTP}(\frac{n}{2}) - G_{LTD}(\frac{n}{2})}{G_{max} - G_{min}}$$

Where $G_{LTP}(n/2)$ and $G_{LTD}(n/2)$ are the intermediate current values of LTP and LTD curves respectively, G_{max} and G_{min} are the maximum and minimum current of the device.

References

1 X. Li, L. Yi, X. Yin, J. Cheng, Q. Xin and A. Song, *npj Flexible Electronics*, 2025, **9**, 57.

2 J. Zeng, L. Hu, Y. Pan, Z. Huang, H. Sun, J. Zeng, X. Xie and H. Chen, *Advanced Functional Materials*, 2025, **35**, 2508292.

3 Y. Dai, G. Chen, W. Huang, C. Xu, C. Liu, Z. Huang, T. Guo and H. Chen, *Science China Materials*, 2024, **67**, 2246-2255.

4 Z. Yang, S. Huo, Z. Zhang, F. Meng, B. Liu, Y. Wang, Y. Ma, Z. Wang, J. Xu, Q. Tian, Y. Wang, Y. Ding, X. Hu, Y. Xie, S. Fan, C. Pan and E. Wu, *Advanced Functional Materials*, 2025, **35**, 2509119.

5 R. Ci, Z. Yin, G. Miao, Y. Wang, G. Liu and F. Shan, *Journal of Materials Chemistry C*, 2025, **13**, 11207-11213.

6 D.-w. Cao, Y. Yan, M.-n. Wang, G.-l. Luo, J.-r. Zhao, J.-k. Zhi, C.-x. Xia and Y.-f. Liu, *Advanced Functional Materials*, 2024, **34**, 2314649.